ACADEMIC PRESS

Available online at www.sciencedirect.com
SCIENCE DIRECT®

Journal of Catalysis 217 (2003) 209–221

JOURNAL OF CATALYSIS

www.elsevier.com/locate/jcat

Microcalorimetric, infrared spectroscopic and DFT studies of CO adsorption on Rh and Rh–Te catalysts

Rong He,[a] Haruhiko Kusaka,[b] Manos Mavrikakis,[a] and James A. Dumesic [a,*]

[a] *Department of Chemical Engineering, University of Wisconsin-Madison, Madison, WI 53706, USA*
[b] *Mitsubishi Chemical Corporation, Yokohama 227-8502, Japan*

Received 4 November 2002; revised 27 December 2002; accepted 7 January 2003

Abstract

Microcalorimetric measurements of the adsorption of CO on a $Rh/0.9Te/SiO_2$ catalyst were performed at 203, 253, and 303 K. The initial heats of CO adsorption were approximately 87 kJ/mol, and this value is much weaker than the value of 160 kJ/mol measured on a Rh/SiO_2 catalyst. Infrared spectra were collected for CO adsorbed on Rh/SiO_2, $Rh/0.7Te/SiO_2$, and $Rh/0.9Te/SiO_2$ catalysts. The primary IR bands were located at frequencies near 2030 cm^{-1} for the $Rh/Te/SiO_2$ catalysts, compared to the higher frequency of 2080 cm^{-1} for CO on Rh/SiO_2. In addition, the intensity of the IR band for CO on the $Rh/Te/SiO_2$ catalysts increased irreversibly when the samples were warmed from 203 to 303 K. Periodic self-consistent DFT–GGA calculations were carried out to study the adsorption of CO on slabs of Rh(111), RhTe(0001), and RhTe($11\bar{2}0$). These calculations show that CO adsorbs strongly on Rh(111), Rh-terminated RhTe(0001), and RhTe($11\bar{2}0$) surfaces, with heats higher than 160 kJ/mol. In contrast, weaker adsorption was calculated for adsorption of CO on Te-terminated RhTe(0001) surfaces, with a heat near 70 kJ/mol. Thus, the Te-terminated RhTe(0001) surface appears to be the best model surface for $Rh/0.9Te/SiO_2$ catalyst, based on the combined results of microcalorimetric measurements and DFT calculations. Adsorption of CO on the hcp site of the Te-terminated RhTe(0001) surface leads to a reconstruction in which the Rh atom bonded to CO is pulled from its position in the second layer to a location above the surface. A lower limit for the activation energy barrier of this CO-induced surface reconstruction is 44 kJ/mol (which corresponds to the barrier of the more exothermic O-induced surface reconstruction). This CO-induced surface reconstruction may be the origin for the experimentally observed increase in the intensity of the IR band for adsorbed CO when $Rh/Te/SiO_2$ samples are warmed from 203 to 303 K in the presence of CO.

Keywords: Microcalorimetry; IR; DFT; Rhodium; Tellurium; Rh–Te alloy; CO; Reconstruction; Kinetics

1. Introduction

Supported Rh–Te catalysts display unique properties for oxidation reactions. For example, Hara et al. have conducted intensive studies of the oxidative diacetoxylation of 1,3-butadiene in the liquid phase using supported Rh–Te catalysts, and these authors have shown that 2-butene-1,4-diol diesters are formed with high activity and selectivity [1]. Takehira et al. [2,3] also showed that while several additives (Te, Se, Bi, and Sb) improved the performance of Pd- and Rh-based catalysts for the acetoxylation of butadiene, the addition of Te caused the most beneficial effects on activity and selectivity. The detailed structures of these Pd–Te and Rh–Te catalysts remain unknown. In addition, intermetallic compounds of Rh show high activity and stereochemical selectivity for oxidative acetoxylation of cyclic conjugated alkadienes to diacetoxycycloalkenes in acetic acid [4], superior to the performance of Pd, Pt, and Ir. More generally, Te-modified transition metal catalysts are known to catalyze various oxidation reactions. In this respect, Mo–Te catalysts, as well as W–Mo–Te and V–Te catalysts oxidize propylene to acrolein and acrylic acid [5]. Carbon-supported Pd–Te catalysts are used for liquid-phase reaction of cyclohexene with acetic acid and oxygen, producing 3-acetoxycyclohexene with 62.8% selectivity [6]. Reaction of 1,3-butadiene with methanol at high pressures of air (100 bar) on a Pd–Te/C catalyst produces 1,2-dimethoxy-3-butene and 1,4-dimethoxy-2-butene [7]. The use of Te as a promoter to carbon-supported noble metal catalysts leads to improved performance in liquid-

* Corresponding author.
E-mail address: dumesic@engr.wisc.edu (J.A. Dumesic).

0021-9517/03/$ – see front matter
doi:10.1016/S0021-9517(03)00020-4

phase oxidation of N-(phosphonomethyl)iminodiacetic acid to N-(phosphonomethyl) glycine by increased oxidation of byproducts (formaldehyde and formic acid) [8].

To our knowledge, detailed surface science studies have not been conducted to understand the chemical properties of metal surfaces modified with Te. Specifically, no literature has been reported to date involving studies of Te-modified Rh single crystal surfaces, and the relatively low melting point of Te (723 K) causes difficulties in preparing such surfaces for studies in UHV systems. We have shown previously that the combination of microcalorimetric measurements, infrared spectroscopy, and density functional theory (DFT) calculations can be used to probe the adsorption of ethylene on PtSn [9], RuSn [10], and PdSn [11]. In the present study, we apply these experimental techniques and theoretical methods to study the RhTe system, with the aim of providing information about surface composition, chemisorptive properties, as well as surface reactivity and stability for $Rh/Te/SiO_2$ catalysts. We found from our experimental measurements that the surface sites on $Rh/Te/SiO_2$ catalysts are significantly different from those on a Rh/SiO_2 catalyst. Importantly, in view of the lack of surface science literature on Rh–Te system, we find that theoretical studies provide a useful means to help understand the observed experimental data for Rh–Te-based catalysts.

We have chosen CO as the main probe molecule in our study, mainly because experimental information is available for CO adsorption on Rh single crystal surfaces and Rh particles supported on various metal oxide supports and because results from DFT calculations are available for CO adsorption on Rh(111) and Rh(211) surfaces. The adsorption of CO on single crystal Rh(111) has been intensively studied by high resolution core level photoemission [12,13], by scanning tunneling microscopy [14], by the combination of HREELS, LEED, and thermal desorption spectroscopy [15], as well as by density functional theory calculations [16,17]. In general, results of experimental studies are in agreement that CO adsorbs preferentially on atop sites at low coverage, whereas three-fold hollow sites are populated at higher coverage. Despite the difficulty of DFT methods in predicting the site preference (atop vs three-fold hollow) of CO adsorption on a few transition metals [18], the results from DFT calculations predicted the same order of site preference as the experimental observations [17]. Adsorption of CO on Rh supported by SiO_2, Al_2O_3, TiO_2 has been studied by infrared spectroscopy [19–24]. The SiO_2 support was shown to have a weaker metal-support effect on Rh, compared with Al_2O_3 and TiO_2 [20,23]. The efficiency of supports in promoting the dissociation of CO on Rh was found to decrease in the order $TiO_2 > Al_2O_3 > SiO_2 > MgO$ at 548 K [24]. CO adsorbs and desorbs molecularly on Rh/SiO_2, whereas dissociation occurs on Rh/Al_2O_3 and Rh/TiO_2 at 296 K [20]. The dissociation of CO on Rh particles of various sizes supported on thin alumina films has been studied, and the maximum extent of CO dissociation takes place on particles containing about 150 Rh atoms [25]. The structure sensitivity of CO dissociation on Rh has been analyzed theoretically, in terms of both thermochemistry and kinetics [16]. In addition, the interaction of CO with supported Rh clusters leads to disruption of Rh crystallites and formation of Rh^+ at 250–423 K, as confirmed by recent STM studies of Rh crystallites supported on TiO_2 [26].

In this work, we have employed infrared spectroscopy to study the interaction of CO with surface sites on Rh/SiO_2 and $Rh/Te/SiO_2$ catalysts. In addition, microcalorimetric studies of the adsorption of CO were conducted to probe the strength of interaction of CO with the surface sites and to determine the number of surface sites. DFT calculations were carried out to investigate the interaction of CO with Rh(111), RhTe(0001), and RhTe($11\bar{2}0$) surfaces. We then combined these DFT results with experimental data to provide information about the surface on the $Rh/Te/SiO_2$ catalysts.

2. Experimental/methods

2.1. Catalyst preparation

The $Rh/Te/SiO_2$ catalysts and the Rh/SiO_2 catalyst with 3 wt% Rh loading were prepared according to the method described by Hara et al. [1]. The support used was silica gel (Cariact), with a surface area of 300 m^2/g and a pore volume of 1 cm^3/g. The support was contacted with an equal volume of a solution containing $RhCl_3$ and/or H_6TeO_6, and the solid was separated from solution via centrifugation, followed by heating in flowing air at 423 K for 5 h (space velocity = 1500 h^{-1}). The dried catalyst was then heated to 573 K in flowing nitrogen, the nitrogen was replaced with hydrogen (space velocity = 750 h^{-1}), and the catalyst was heated to 673 K and held for 2 h. Two $Rh/Te/SiO_2$ catalysts were made with nominal atomic ratios of Te:Rh equal to 0.9 and 0.7.

The $Rh/Te/SiO_2$ catalysts and the Rh/SiO_2 catalyst have been characterized with inductively coupled plasma–atomic emission spectrometry (ICP–AES) and transmission electron microscopy (TEM). For the purpose of ICP–AES, the catalysts were dissolved in aqua regia, then the solution was filtered and the filtrate was analyzed for Rh and Te concentrations. The Rh loading of Rh/SiO_2, $Rh/0.7Te/SiO_2$, and $Rh/0.9Te/SiO_2$ catalysts are 2.76, 2.70, and 3.11 wt%, respectively. The atomic ratios of Te:Rh are 0.71 and 0.92 on $Rh/0.7Te/SiO_2$ and $Rh/0.9Te/SiO_2$, respectively. Transmission electron microscopy was performed using a Hitachi H-9000UHR microscope with top-entry goniometer at 300 keV acceleration voltage. The point-to-point resolution was 0.18 nm. Samples for TEM were prepared by ultrasonic dispersion of catalysts in ethanol and subsequent deposition onto copper TEM grids with holey carbon support films.

2.2. Microcalorimetry

Microcalorimetric measurements were performed using a Setaram BT2.15D heat-flux calorimeter. Details of the procedures for microcalorimetric measurements can be found elsewhere [27,28]. In short, each sample was first treated in flowing hydrogen at 673 K for 8 h, followed by treatment in flowing helium for 0.5 h. Both gases were of ultrahigh purity. The sample was then sealed in a Pyrex capsule, and the capsule was loaded into a set of calorimetric cells [28]. After the sample has reached thermal equilibrium with calorimeter, the capsule was broken and microcalorimetric measurements were taken by sequentially introducing small doses (1–10 μmol) of probe molecules onto the sample. The heat signal was recorded as a function of time, and this signal was integrated to obtain the energy released per dose. Volumetric measurements were made to determine the amount of gas adsorbed during the dose, using the dosing pressure, equilibrium pressure, system volumes, and temperatures. The differential heat (kJ/mol), defined as the negative of the enthalpy change of adsorption per mole of gas adsorbed, was then calculated for each dose by dividing the heat released by the amount adsorbed.

The maximum apparent leak rate of the calorimetric cells and the gas handling system, measured by a Baratron capacitance manometer ($\pm 0.5 \times 10^{-4}$ Torr), was 10^{-6} Torr/min in a system volume of ~ 70 cm^3 (i.e., 10^{-6} μmol/min). The contamination over a typical run (~ 5 h) is less than 10^{-3} μmol, which is low compared with the total uptake of $Rh/0.9Te/SiO_2$ sample (ca. 5 μmol).

2.3. Infrared spectroscopy

The infrared spectroscopy cell used in this work allows collection of in-situ IR spectra at temperatures from 153 to 673 K [9]. Catalyst samples (ca. 20 mg) were pressed into self-supporting pellets (1.3 cm^2) and loaded into the IR cell. The samples were then reduced in flowing H_2 for 8 h at 673 K, and subsequently purged in flowing He for 1.5 h at 673 K. The IR cell was connected to a high vacuum system and placed in the infrared spectrometer (Mattson Galaxy Series FTIR 5000). The cell was evacuated to 0.2 Torr of He to facilitate heat conduction during cooling to subambient temperatures. Reference spectra were collected at 303 and 203 K, CO was then dosed onto the pellet at 203 K until the CO pressure reached 3 Torr, and an IR spectrum was collected. The sample was subsequently warmed to 303 K in 3 Torr of CO, and another spectrum was collected, after which CO was evacuated from the cell for 20 min at 303 K and another spectrum was collected. In several experiments, IR spectra were subsequently collected after the sample was next cooled in CO to 203 K, and then after warming the sample again to 303 K. These spectra were collected to check the reversibility of changes in spectra caused by changes in sample temperature for the 3% $Rh/0.7Te/SiO_2$ catalyst.

All infrared spectra were collected in the absorbance mode using 1000 scans with a resolution of 2 cm^{-1}. Spectra reported herein are weight-averaged difference spectra, corresponding to IR spectra of the sample plus adsorbate minus the IR spectrum of the clean sample at the same temperature, normalized by the amount of sample used to make the pellet.

2.4. DFT calculations

Self-consistent, gradient-corrected, periodic DFT calculations were carried out to investigate the interaction of CO with Rh(111) [16,17], RhTe(0001), and RhTe($11\bar{2}0$) surfaces. The compound RhTe has a more simple crystal structure compared with Rh_3Te_2 and Rh_3Te_4 [29]. In this study, we used four layer slabs for RhTe(0001) and RhTe($11\bar{2}0$), periodically repeated in a super cell geometry with four equivalent layers of vacuum between successive metal slabs. The structures of all slabs studied are shown in Fig. 1. The RhTe(0001) slab is a layered structure with alternating layers of pure Rh and Te; thus, two types of surfaces (Rh-terminated and Te-terminated) are possible for adsorption, as shown in Figs. 1b and 1c. A 2×2 unit cell was used in most calculations, corresponding to $1/4$ ML coverage, whereas a 3×3 unit cell, corresponding to $1/9$ ML coverage, was used for selected calculations on RhTe(0001). Adsorption is allowed on one of the two exposed surfaces, and the electrostatic potential is adjusted accordingly [30]. In all cases, the bottom two layers are fixed at their bulk positions, whereas the top two layers, together with the adsorbate species, were allowed to relax.

The equilibrium lattice constant determined from DFT calculations for Rh is 3.83 Å [16,17], which is within 1% of the experimental value of 3.797 Å [31]. The equilibrium lattice constant of the hexagonal RhTe unit cell was determined by fixing the axial ratio c/a at the experimental value (1.418) and then minimizing the electronic energy by varying the lattice constant. The calculated value of the lattice constant is 4.16 Å, and the corresponding experimental value is 3.99 Å [32].

All DFT calculations were performed using DACAPO [33]. In these calculations, ultrasoft pseudopotentials [34] are used to describe ionic cores, and the Kohn–Sham one-electron valence states are expanded in a basis of plane waves with kinetic energies below 25 Ry. The exchange-correlation energy and potential are described by the generalized gradient approximation (PW91) [35,36]. The self-consistent PW91 density is determined by iterative diagonalization of the Kohn–Sham Hamiltonian, Fermi-population of the Kohn–Sham states ($k_BT = 0.1$ eV), and Pulay mixing of the resulting electronic density [37]. All reported binding energies are calculated using the PW91 functional, and these energies have been extrapolated to $k_BT = 0$ eV. We have used the nonspin polarized version of the exchange correlation functional. The surface Brillouin zone is sampled at 18 special **k** points. In all cases, con-

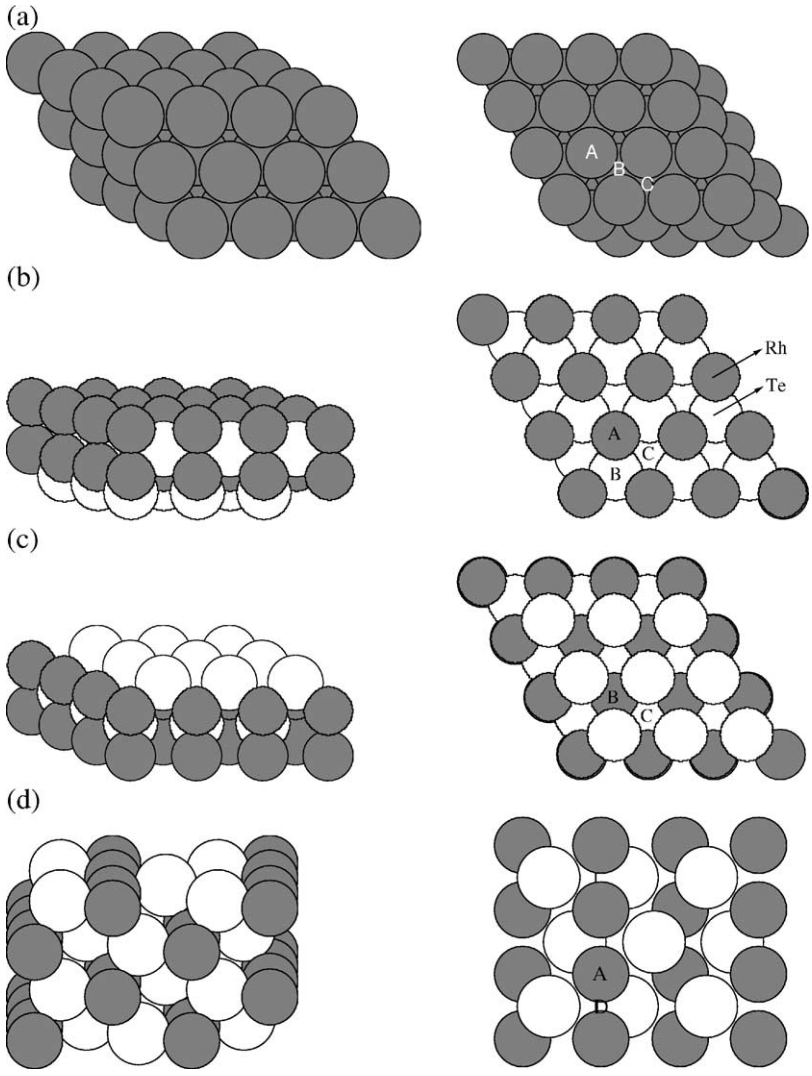

Fig. 1. Side and top views of (a) Rh(111), (b) Rh-terminated RhTe(0001), (c) Te-terminated RhTe(0001), and (d) RhTe(11$\bar{2}$0) slabs. The gray-filled circles represent Rh atoms; the white circles represent Te atoms.

vergence has been confirmed with respect to the number of metal layers, cut-off energy, and **k** point set.

The C–O stretching frequency of adsorbed CO is calculated using the harmonic oscillator approximation [38]. Based on the optimized structure on a relaxed surface, a series of static calculations are performed for adsorbed CO, in which the C–O bond is stretched or compressed to up to 1% of its equilibrium length. The resultant data points for binding energy versus bond length are then fitted to a parabola $E = k(x - b)^2/2$, where k is related to the vibrational frequency of the harmonic oscillator by

$$\nu = \sqrt{k/M}\,/2\pi,$$

M being the reduced mass of the CO molecule.

Due to the extremely demanding character of the calculation of the activation energy barrier for CO-induced surface reconstruction, we studied the corresponding process with an O atom, which is considerably more tractable. Using a Brønsted–Evans–Polanyi relationship [39,40], we then estimated the barrier for the CO-induced surface reconstruction. In particular, we performed a series of constrained optimizations for adsorption of an O atom on the hcp site of Te-terminated RhTe(0001), where the height of the Rh atom relative to bottom layer representing reaction coordinate is constrained and all other degrees of freedom are optimized. The transition state is characterized by the configuration with the highest energy along the reaction coordinate and a simultaneous change in the sign of residual force on the Rh atom along the reaction coordinate.

3. Results

3.1. Experimental studies

Fig. 2a shows microcalorimetric results for the adsorption of CO on the 3% $Rh/0.9Te/SiO_2$ catalyst at 203, 253, and 303 K. The initial heats of adsorption at these three

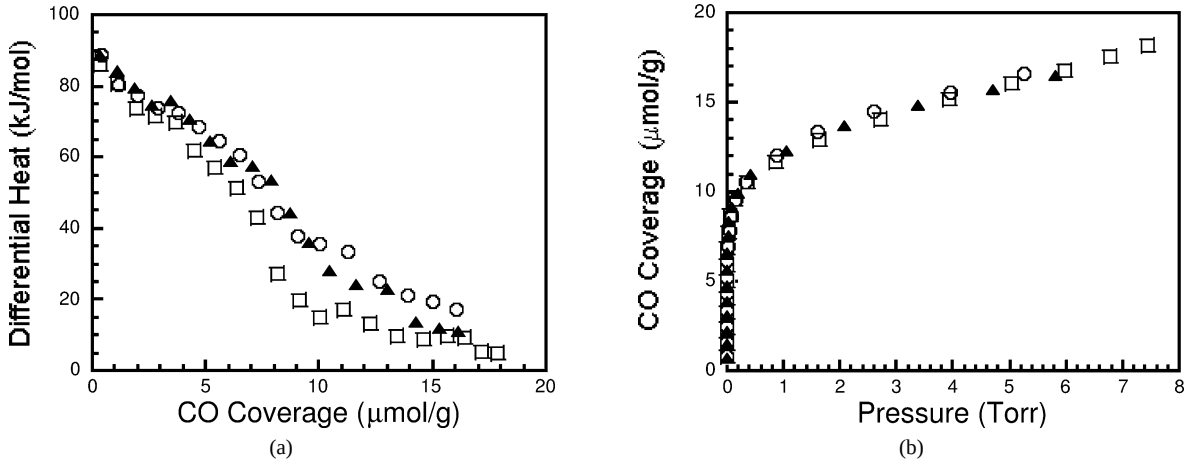

Fig. 2. (a) Differential heat versus adsorbate coverage and (b) adsorption isotherms for CO adsorption on 3% $Rh/0.9Te/SiO_2$ at 203 K (□), 253 K (▲), and 303 K (○).

temperatures are approximately equal to 87 kJ/mol. For adsorption at all three temperatures, the heat of adsorption decreases continuously as the uptake increases. The curve of heat versus coverage at 203 K lies under those at 253 and 303 K. The isotherms at three temperatures overlap with each other (Fig. 2b), and the monolayer uptake of CO was about 12 μmol/g.

For comparison, microcalorimetric results for the adsorption of CO on a 3% Rh/SiO_2 catalyst at 403 K are shown in Fig. 3. The initial heat of adsorption is 160 kJ/mol, followed by a plateau of nearly constant heat at 140 kJ/mol. The saturation uptake of CO is 60 μmol/g. Thus, the addition of Te lowers substantially both the initial heat of CO adsorption and the uptake, indicating both electronic and geometric effects of Te. Smedh et al. have reported that the isosteric heat of adsorption of CO on Rh(111) decreases from just above 1.5 eV (145 kJ/mol) to 1.3 eV (125 kJ/mol) as the coverage increases from 0.18 ML to about 0.3 ML [12]. The energy change for adsorption of CO on Rh(111) has also been measured at low coverages to be 1.65 eV (159 kJ/mol) [41]. The results from our microcalorimetric measurements of CO adsorption on Rh/SiO_2 are thus consistent with results from studies using single crystal surfaces.

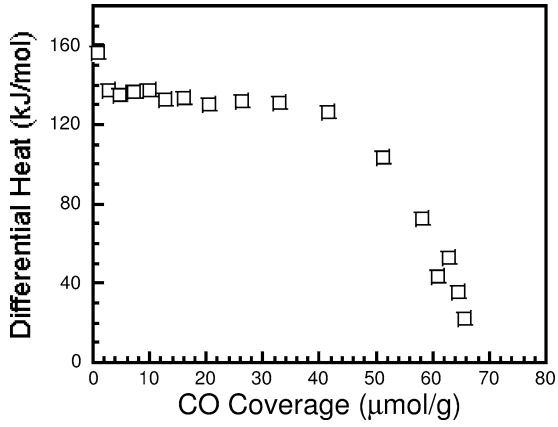

Fig. 3. Differential heat versus adsorbate coverage for CO adsorption on 3% Rh/SiO_2 at 403 K.

Representative transmission electron micrographs of Rh/SiO_2, $Rh/0.7Te/SiO_2$, and $Rh/0.9Te/SiO_2$ catalysts are shown in Figs. 4a–4c, respectively. The $Rh/0.7Te/SiO_2$ catalyst had a smaller average metallic particle size than the Rh/SiO_2 catalyst (2.5 versus 2.9 nm), whereas the $Rh/0.9Te/SiO_2$ catalyst had a slightly larger average metallic particle size than the Rh/SiO_2 catalyst (3.3 versus 2.9 nm). Therefore, these small changes in metallic particle size caused by the addition of Te to Rh/SiO_2 are not responsible for the significantly lower CO uptake measured on the $Rh/0.9Te/SiO_2$ catalyst (by 80%).

Infrared spectra of CO adsorbed on 3% $Rh/0.9Te/SiO_2$ are shown in Fig. 5a. The adsorption of CO on this catalyst at 203 K with 3 Torr CO in gas phase leads to two overlapping bands at 2031 and 2057 cm^{-1}. The intensities of both bands increased when the sample was warmed to 303 K in 3 Torr gas-phase CO, and the band at 2031 cm^{-1} shifted to 2035 cm^{-1}. Evacuating CO from the cell for 20 min attenuated the intensity of the band at 2057 cm^{-1} more than the band at 2031 cm^{-1}, which suggests that the band at 2057 cm^{-1} corresponds to weaker adsorption of CO. No band was observed in the 1800–1900 cm^{-1} frequency range.

Fig. 5b shows infrared spectra of CO adsorbed on 3% $Rh/0.7Te/SiO_2$. Exposing this sample to 3 Torr of CO at 203 K leads to a band at 2022 cm^{-1}, with a shoulder at 2051 cm^{-1}. Upon warming the sample to 303 K, the intensity of the band at 2022 cm^{-1} increased considerably compared to the band at 203 K. The shoulder at 2051 cm^{-1} is still distinguishable at 303 K. To test whether this intensity change is reversible relative to changes in temperature, the sample was cooled and warmed again in CO, and the two corresponding spectra collected at 203 and 303 K are similar to the spectrum collected initially at 303 K. Evacuating CO from the cell at 303 K slightly attenuated the intensity of the band at 2022 cm^{-1}.

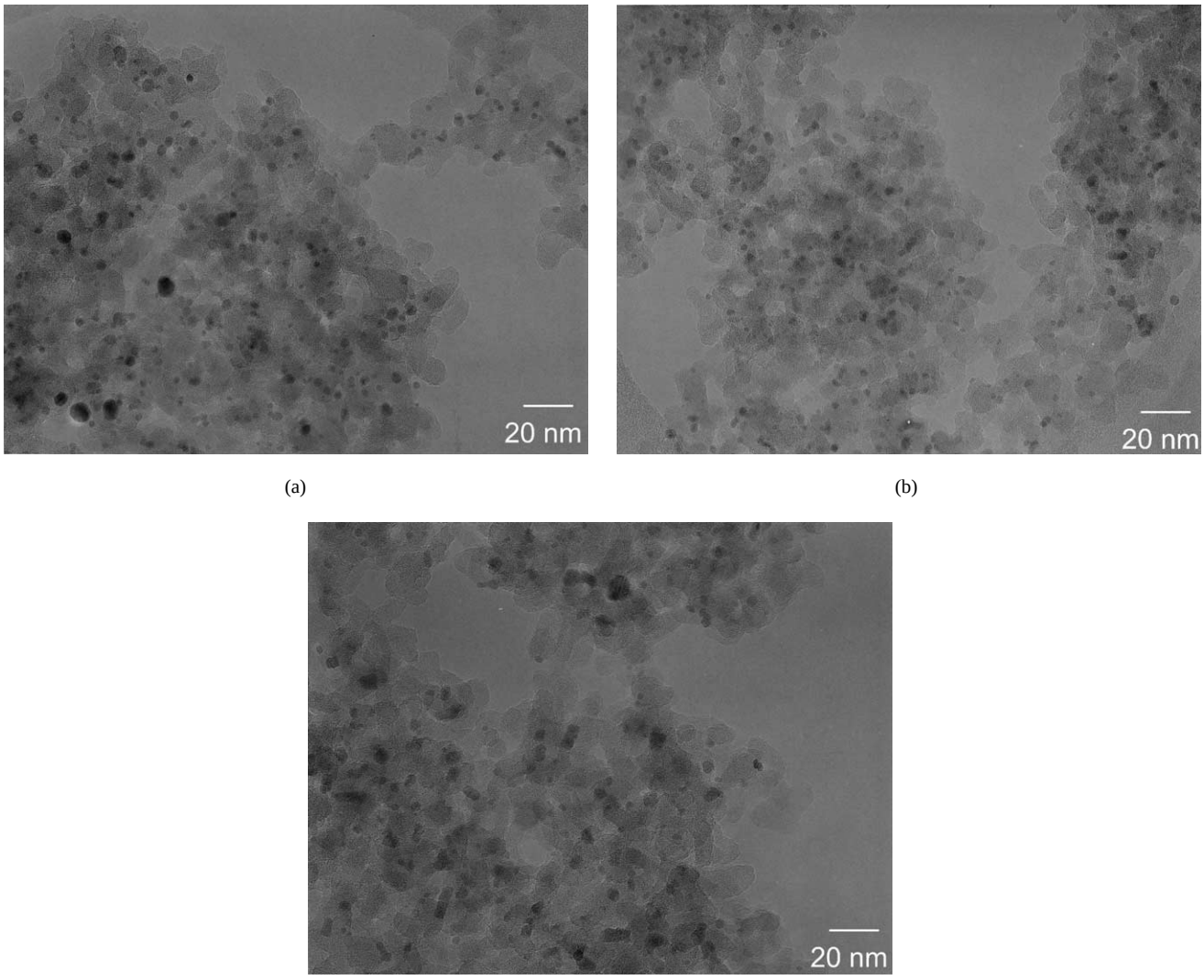

(a) (b)

(c)

Fig. 4. TEM images of (a) 3% Rh/SiO_2, (b) 3% $Rh/0.7Te/SiO_2$, and (c) 3% $Rh/0.9Te/SiO_2$ catalysts.

Fig. 5c shows infrared spectra of CO adsorbed on 3% Rh/SiO_2. After the sample was exposed to 3 Torr of CO at 203 K, a sharp band at 2080 cm^{-1} and a broad band near 1918 cm^{-1} were detected. Warming the sample to 303 K did not change the intensities of the bands noticeably. Evacuating CO from the cell for 20 min slightly decreased the intensity of the band at 2080 cm^{-1}. The band located at 2080 cm^{-1} is assigned to linear-bonded CO on metallic Rh, whereas the band near 1918 cm^{-1} band is assigned to multi/bridge-bonded CO on Rh [20]. As shown next, DFT calculations predict a vibrational frequency of 2072 cm^{-1} for CO adsorbed on an atop site of Rh(111).

3.2. DFT calculations

The interactions of CO with various sites on RhTe(0001), RhTe(11$\bar{2}$0), and Rh(111) slabs were studied mainly with 2×2 unit cells. Adsorption of CO on the Rh-terminated RhTe(0001) surface can occur on three types of surface sites shown in Fig. 1b: atop site (A); hcp site (B), which consists of three-fold Rh site with underlying Te atom; and fcc site (C), which consists of three-fold Rh site over three-fold Te site in the second layer. Adsorption of CO on the Te-terminated RhTe(0001) surface can occur on two types of surface sites shown in Fig. 1c: hcp site (B), which consists of three-fold Te site with underlying Rh atom and fcc site (C), which consists of three-fold Te site over three-fold Rh site in the second layer. On the RhTe(11$\bar{2}$0) slab, atop and bridge sites are available for CO adsorption, labeled as A and D in Fig. 1d, respectively. Results of DFT calculations for CO adsorption on atop, hcp, and fcc sites of Rh(111) slab, labeled as A, B, and C in Fig. 1a, are also reported for comparison [16,17]. The adsorption of CO on the hcp site of Te-terminated RhTe(0001) was further studied with a 3×3 unit cell to reduce symmetry limitations on the surface reconstruction induced by CO adsorption.

Calculated energy changes for adsorption of CO on Rh- and Te-terminated RhTe(0001), RhTe(11$\bar{2}$0), and Rh(111)

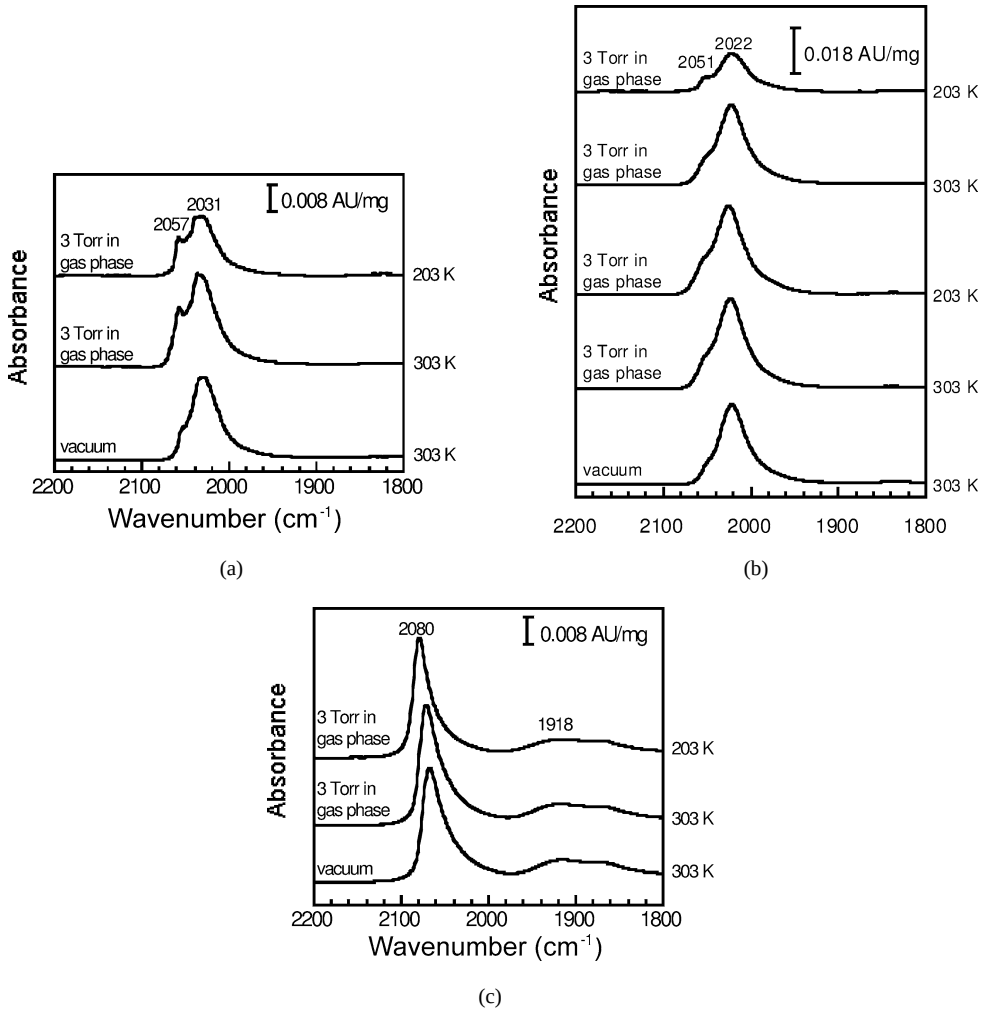

Fig. 5. Infrared spectra for CO adsorption on (a) 3% Rh/0.9Te/SiO_2, (b) 3% Rh/0.7Te/SiO_2, and (c) 3% Rh/SiO_2.

surfaces are listed in Table 1. The energy changes for CO adsorption on atop, hcp, and fcc sites of the Rh-terminated RhTe(0001) surface are −246, −247, and −264 kJ/mol, respectively. The corresponding values for CO adsorption on atop, hcp, fcc sites of Rh(111) surface are −196, −192, and −182 kJ/mol, respectively [16,17]. Results of DFT calculations by Zhang et al. [42] predicted the energy change for adsorption of CO on atop sites of Rh(111) to be −1.86 eV (−179 kJ/mol). Therefore, the Rh-terminated RhTe(0001) surface is an even more reactive surface for CO adsorption than Rh(111). In contrast, the energy changes for adsorption of CO on hcp and fcc sites of Te-terminated RhTe(0001) surface are only −58 and −14 kJ/mol, respectively. The energy changes for CO adsorption on atop and bridge sites of RhTe(11$\bar{2}$0) are intermediate between the values for the Rh-terminated and Te-terminated RhTe(0001) surfaces, with values equal to −167 and −184 kJ/mol, respectively.

Table 1
Results from DFT calculations for changes in electronic energies (kJ/mol) for interaction of CO with relaxed Rh(111),[a] RhTe(0001), and RhTe(11$\bar{2}$0) slabs. The reference zero corresponds to gas-phase CO at infinite separation from the slabs

Sites	Rh-terminated RhTe(0001)	Te-terminated RhTe(0001)	RhTe(11$\bar{2}$0)	Rh(111)
atop	−246		−167	−196
hcp	−247	−58;[b] −69[c]		−192
fcc	−264	−14		−182
bridge			−184	

[a] M. Mavrikakis, M. Baumer, H.-J. Freund, J.K. Nørskov, Catal. Lett. 81 (2002) 153. M. Mavrikakis, J. Rempel, J. Greeley, L.B. Hansen, J.K. Nørskov, J. Chem. Phys. 117 (2002) 6737.

[b] Energy change calculated at $\theta = 1/4$ ML with Rh atom of hcp site under surface Te layer.

[c] Energy change calculated at $\theta = 1/9$ ML with Rh atom of hcp site pulled above surface Te layer.

Fig. 6a shows side and top views of CO adsorbed on the atop site of Rh-terminated RhTe(0001). No significant lateral relaxation of Rh or Te atoms is observed. The C–O and Rh–C bond lengths are 1.18 and 1.83 Å, respectively. We note that the calculated C–O bond length for gas-phase molecule is 1.156 Å, compared with the experimental value of 1.128 Å [43]. The Rh atom coordinated to CO has an upward shift of 0.08 Å compared with the other three Rh

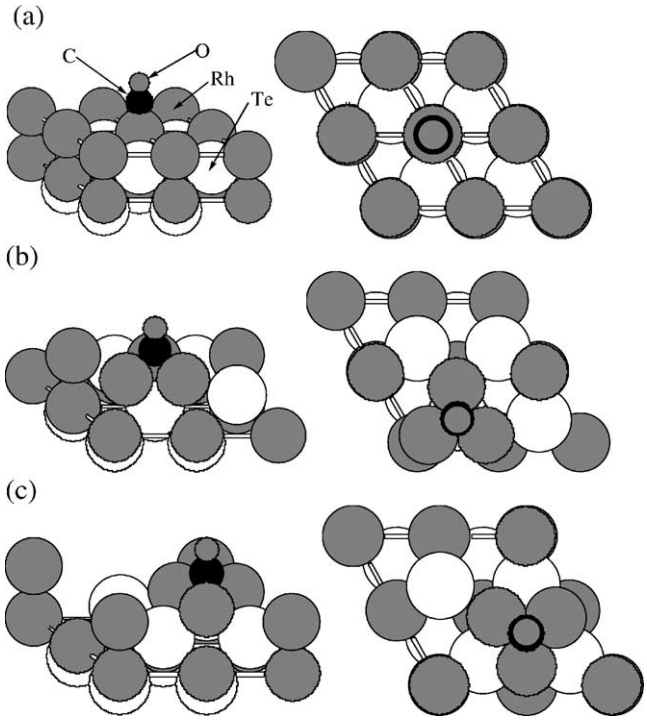

Fig. 6. Side and top views of the 2×2 unit cell for adsorption of CO on the (a) atop site, (b) hcp site, and (c) fcc site on Rh-terminated RhTe(0001). The large gray circle is the Rh atom; the large white circle is the Te atom; the medium black circle is the C atom; and the small gray circle is the O atom.

atoms in the unit cell. For comparison, CO adsorbed on the atop site of Rh(111), leads to C–O and Rh–C bond lengths of 1.17 and 1.83 Å, respectively, and the upward shift of the Rh atom coordinated to CO is 0.2 Å. In contrast to the aforementioned two cases, adsorption of CO on three-fold sites of Rh-terminated RhTe(0001) leads to major surface reconstructions, as shown in Fig. 6b (hcp site) and Fig. 6c (fcc site). On the hcp site, the lateral movements of the three-fold Rh atoms toward CO are 0.74, 0.74, and 0.78 Å (where all lateral movements are calculated by comparison with bulk-truncated positions), making the corresponding Rh–C bond lengths equal to 2.07, 2.07, and 2.08 Å. In addition, the underlying Te atom in the hcp site has a downward shift of 0.80 Å, compared to the other three Te atoms in the second layer. On the fcc site, the lateral movements of the three-fold Rh atoms toward CO are 0.72, 0.74, and 0.87 Å, and lengths of the Rh–C bonds are 2.06, 2.06, and 2.05 Å. The underlying three-fold Te atoms all have a downward shift of 0.08 Å relative to the other Te atom in the second layer. The C–O bond lengths for adsorption on hcp and fcc sites of Rh-terminated RhTe(0001) are both 1.22 Å.

Fig. 7a shows side and top views of CO adsorbed on the hcp site of the Te-terminated RhTe(0001) slab. The C atom of CO is bonded to the underlying Rh atom in the hcp site, with a Rh–C bond length of 1.79 Å. This Rh atom bonded to CO has an upward shift of 0.68 Å compared to the other Rh atoms in the second layer. The three-fold Te

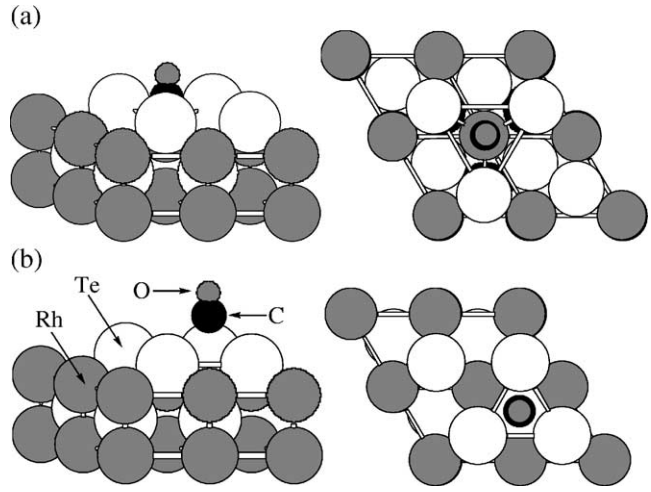

Fig. 7. Side and top views of the 2×2 unit cell for adsorption of CO on the (a) hcp site and (b) fcc site on Te-terminated RhTe(0001). The large gray circle is the Rh atom; the large white circle is the Te atom; the medium black circle is the C atom; and the small gray circle is the O atom. The large black circle in (b) represents the original position of the Te atoms.

atoms in the top layer are displaced laterally away from CO by 0.29, 0.27, and 0.29 Å. The C–O bond length in this geometry is 1.18 Å. We note that this geometry is not able to fully minimize the electronic energy within 200 geometry optimization steps, since the Rh atom in the hcp site continues to move up slowly during optimization. This observation suggests that the Rh atom may be eventually pulled up to the surface by CO, reminiscent of the formation of a Rh–CO surface carbonyl species [44]. This situation will be explored more fully below for adsorption of CO on the hcp site of a Te-terminated RhTe(0001) slab with a 3×3 unit cell. Adsorption of CO on fcc sites of the Te-terminated RhTe(0001) surface does not induce significant relaxation in the top two layers of the slab (shown in Fig. 7b), which is consistent with the weak adsorption of CO on this site (i.e., -14 kJ/mol).

Adsorption of CO on atop and bridge sites of RhTe($11\bar{2}0$) does not result in major surface reconstruction, as shown in Fig. 8. On the atop site, the Rh atom coordinated to CO has an upward shift of 0.21 Å, compared with the other Rh atom in the same layer. On bridge sites, the CO molecule is displaced laterally away from the site center by 0.39 Å, possibly because of repulsion by the nearby Te atom. The C–O bond is tilted 8° away from the surface normal. The lengths of the Rh–C and C–O bonds for adsorption of CO on various RhTe slabs, calculated with 2×2 unit cells, are summarized in Table 2.

The observation that it was difficult to find the optimized geometry for CO adsorbed on the hcp site of the Te-terminated RhTe(0001) surface suggests that the 2×2 unit cell may not be sufficient due to symmetry limitations for this case where significant surface reconstruction is induced by CO. Accordingly, we further investigated CO adsorption on hcp sites of Te-terminated RhTe(0001) surface using a 3×3 unit cell. This calculation reached a reasonably

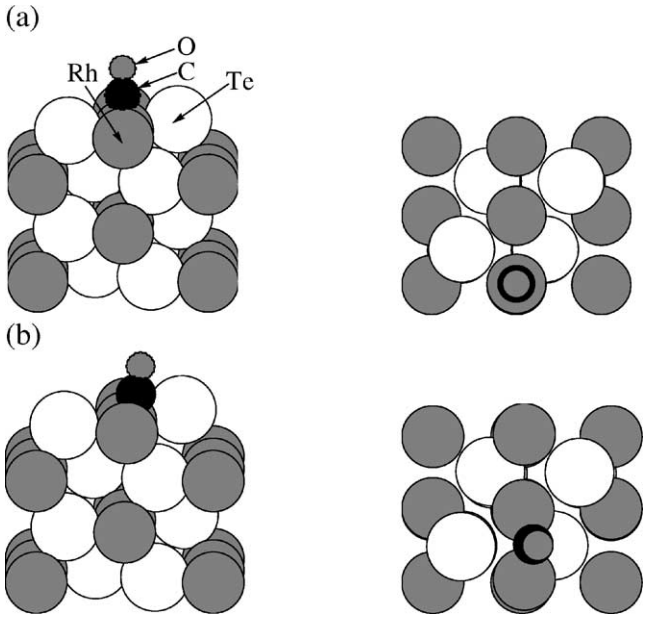

Fig. 8. Side and top views of the 2×2 unit cell for adsorption of CO on the (a) atop site and (b) bridge site on RhTe($11\bar{2}0$). The large gray circle is the Rh atom; the large white circle is the Te atom; the medium black circle is the C atom; and the small gray circle is the O atom.

converged geometry (Fig. 9a), but it was not able to fully converge within a reasonable number of geometry optimization steps (e.g., 110 steps), and the continued upward movement of Rh atom was also observed. The energy change for CO adsorption is -52 kJ/mol, which is close to the value of -58 kJ/mol obtained with the 2×2 unit cell. When the initial guess for the geometry corresponded to the situation where the Rh bonded to CO was completely pulled to a position above the surface, then the calculation was able to fully converge, leading to the geometry shown in Fig. 9b. The corresponding energy change for CO adsorption is -69 kJ/mol. Therefore, the CO-induced surface reconstruction, leading to movement of the underlying Rh atom in the hcp site to a position on the surface, strengthens the bonding of CO by about 17 kJ/mol. As shown in Fig. 9a, partial reconstruction of the surface (formed from initial geometries where all Rh atoms are below the surface) leads to an upward shift of the Rh atom bonded to CO by 0.61 Å compared with the other Rh atoms in the second layer. As seen in Fig. 9b, the completed reconstruction of the surface causes the Rh atom to be completely scavenged by CO, and the Rh atom bonded to CO is displaced by 1.9 Å above the other Rh atoms in the second layer. In both cases, the three-fold Te atoms in the top layer surrounding the hcp site are displaced laterally away from CO to a similar extent, i.e., by 0.26, 0.31, and 0.34 Å.

Table 2
Bond lengths (Å) from DFT calculations for interaction of CO with Rh-terminated and Te-terminated RhTe(0001) surface and RhTe($11\bar{2}0$) surface studied at $\theta = 1/4$ ML

Bond	Slab	atop	hcp	fcc	Bridge
C–Rh	Rh-terminated RhTe(0001)	1.83	2.07, 2.07, 2.08	2.06, 2.06, 2.05	
	Te-terminated RhTe(0001)		1.79	4.30, 4.32, 4.33	
	RhTe($11\bar{2}0$)	1.82			1.97, 1.98
C–O	Rh-terminated RhTe(0001)	1.18	1.22	1.22	
	Te-terminated RhTe(0001)		1.18	1.16	
	RhTe($11\bar{2}0$)	1.17			1.19

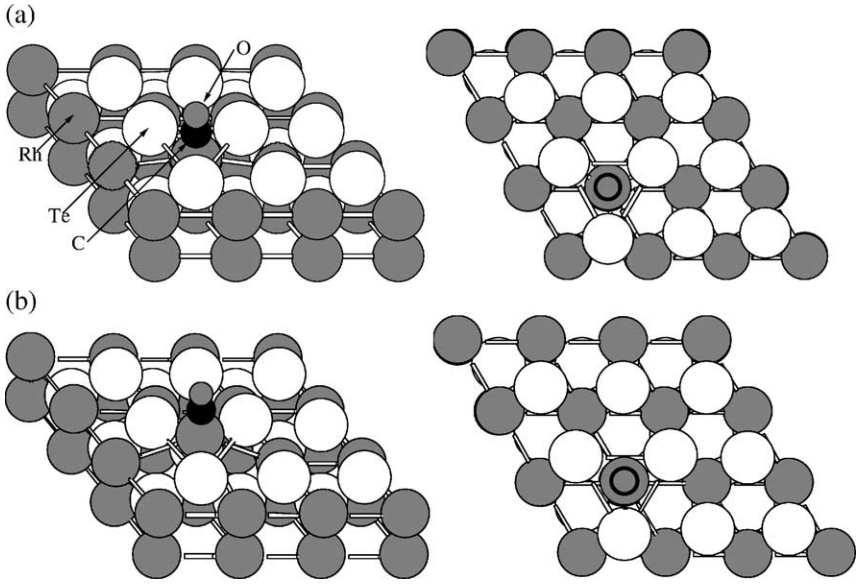

Fig. 9. Side and top views of the 3×3 unit cell for adsorption of CO on hcp site of Te-terminated RhTe(0001) surface with (a) Rh atom of the hcp site remains under the surface Te atoms and (b) Rh atom of the hcp site pulled above the surface Te atoms. The large gray circle is the Rh atom; the large white circle is the Te atom; the medium black circle is the C atom; and the small gray circle is the O atom.

Based on these results for CO adsorbed on various sites of different slabs, specific sites were selected for DFT calculations of C–O vibrational frequencies. In particular, C–O vibrational frequencies were determined for CO adsorbed on the atop site of Rh(111), the fcc site of Te-terminated RhTe(0001) surface, and the hcp site of Te-terminated RhTe(0001) surface with the Rh atom coordinated to CO in a position above the surface. The vibrational frequencies for CO adsorbed at these sites were calculated to be 2072, 2105, and 1974 cm^{-1}, respectively.

As just presented, it was difficult to find the optimized geometry for CO adsorbed on the hcp site of the Te-terminated RhTe(0001) surface, and the energy was lower when the Rh atom bonded to CO was moved to a position on the surface. These results suggested that the movement of this Rh atom to the surface may be an activated process. Accordingly, DFT calculations were conducted on the 3×3 unit cell to estimate the activation energy barrier for a similar process in which the Rh atom is pulled to the surface upon interaction with an oxygen atom. Two stable structures were found after optimization with no constraints, i.e., geometries with the Rh atom remaining in the second layer and with the Rh atom moved on the surface, and the later geometry is energetically more favorable than the former geometry by 45 kJ/mol. The activation energy barrier for surface reconstruction induced by interaction of an oxygen atom with the hcp site of Te-terminated RhTe(0001) was calculated to be 44 kJ/mol. Fig. 10 shows a plot of energy (relative to the gas-phase O atom) versus the constrained height of the Rh atom (with respect to the bottom of the slab) as the reaction coordinate. We note that CO-induced surface reconstruction leads to a stabilization of CO by 17 kJ/mol (3×3 unit cell), and O-induced surface reconstruction leads to a stabilization of O by 45 kJ/mol (3×3 unit cell). Since the surface reconstruction induced by CO is less exothermic than the reconstruction induced by O atoms, we suggest that the less favorable, CO-induced surface reconstruction will have an activation energy barrier of at least 44 kJ/mol.

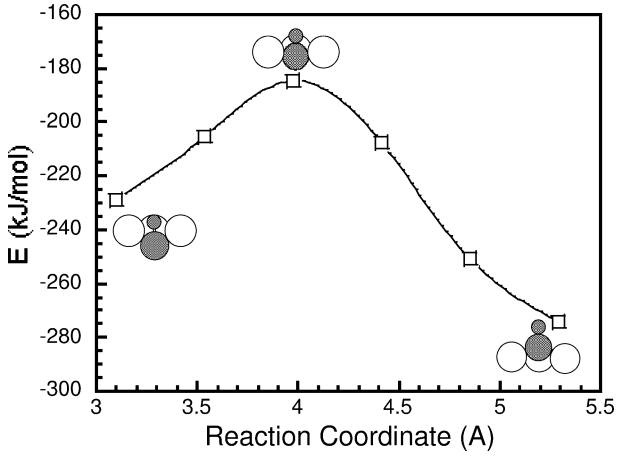

Fig. 10. Plot of energy vs reaction coordinate (height of the Rh atom in hcp site relative to bottom layer of the slab) for the adsorption of O on the hcp site of Te-terminated RhTe(0001) surface. The reference zero corresponds to gas-phase O atom at infinite separation from the slab. Snapshots are side views of the hcp site; the large white circle is the Te atom; the large gray circle is the Rh atom; and the small gray circle is the O atom.

4. Discussion

Results from DFT calculations for CO adsorption on Rh(111) predict that adsorption on the atop site is more favorable than on the hcp site by 4 kJ/mol. This result is consistent with experimental observations for Rh(111) single crystal surfaces that adsorption of CO favors atop sites at low coverage [12–15]. In contrast, our results indicate that for the Rh-terminated RhTe(0001) surface, the fcc site is most favorable for CO adsorption (−264 kJ/mol), compared with atop and hcp sites (−246 and −247 kJ/mol, respectively). Results for CO adsorption on the Te-terminated RhTe(0001) surface show that adsorption on the hcp site is more favorable than the fcc site by 44 kJ/mol. We note, however, that the hcp site for this surface resembles an atop site for CO adsorption, since a Rh atom from the second layer is pulled to the surface upon coordination with adsorbed CO. In general, the results from our DFT calculations indicate that adsorption of CO on the Rh-terminated RhTe(0001) surface is strengthened with respect to adsorption of CO on Rh(111), whereas adsorption of CO on the Te-terminated RhTe(0001) surface is significantly weakened with respect to Rh(111). We attribute the strengthening of CO adsorption on the Rh-terminated RhTe(0001) surface (compared with Rh(111) surface) to the effect of strain [45], noticing that the distances between nearest Rh atoms at the top layer of the Rh-terminated RhTe(0001) and Rh(111) are 4.16 and 2.71 Å, respectively.

Results from microcalorimetric measurements for the heat of CO adsorption on the 3% Rh/SiO_2 catalyst give an initial value of −160 kJ/mol at 403 K, which is in agreement with results from DFT calculations on the Rh(111) surface equal to −196 kJ/mol for the atop site, −192 kJ/mol for the hcp site, and −182 kJ/mol for the fcc site. Infrared spectra of CO on this catalyst provide spectroscopic evidence that both atop sites and three-fold hollow/bridge sites are populated by CO on this catalyst. Microcalorimetric measurements on the 3% $Rh/0.9Te/SiO_2$ catalyst show that bonding of CO with the surface of this catalyst is considerably weaker compared to Rh/SiO_2, with an initial heat of −87 kJ/mol at room temperature. Therefore, the addition of Te to Rh leads to a significant decrease in the initial heat of CO adsorption (i.e., by 72 kJ/mol).

Among the Rh–Te surfaces we have studied with DFT calculations, Rh-terminated RhTe(0001) is the most reactive surface for CO bonding; therefore, it is unlikely that the surface of the 3% $Rh/0.9Te/SiO_2$ catalyst consists predominantly of Rh-terminated RhTe(0001) surfaces. The bonding strength of CO on the RhTe($11\bar{2}0$) surface is comparable with Rh(111) surface. Accordingly, it is also unlikely that the surface of the 3% $Rh/0.9Te/SiO_2$ catalyst consists of

significant amounts RhTe($11\bar{2}0$) surfaces. In contrast, the results of DFT calculations indicate that adsorption of CO on the hcp and fcc sites of Te-terminated RhTe(0001) surface are considerably weaker than adsorption of CO on Rh(111). Consequently, these DFT results combined with the results of microcalorimetric measurements suggest that the 3% $Rh/0.9Te/SiO_2$ catalyst is likely to have a Te-enriched surface, such as the Te-terminated RhTe(0001) surface. In fact, the surface energy of Te is expected to be lower than that for Rh, since the enthalpies of vaporization of Te and Rh at their boiling points are 114.1 and 494 kJ/mol, respectively [43], leading to enrichment of the surface with Te.

The addition of Te to 3% Rh/SiO_2 lowers not only the initial heat, but also the total uptake for CO adsorption. In particular, the saturation CO uptake on 3% $Rh/0.9Te/SiO_2$ is only about 20% of the uptake on the 3% Rh/SiO_2 catalyst, despite the same Rh loading and similar metal particle sizes. On a Te-enriched surface, the Te atoms block a considerable fraction of the metal surface. For example, on the Te-terminated RhTe(0001), the hcp sites are the only sites that lead to significant heats of CO adsorption, and these sites account for only 25% of the metal surface area.

Adsorption of CO on 3% Rh/SiO_2 yields a sharp band at 2080 cm^{-1} and a broad band ca. 1918 cm^{-1}, corresponding to linear-bonded and multi/bridge-bonded CO on metallic Rh. The absence of dicarbonyl species on the Rh/SiO_2 catalyst (corresponding to bands at 2100 and 2030 cm^{-1}) may be related to the relatively high loading of Rh (3 wt%), and the short time in contact with CO at 303 K (< 30 min), and/or the fact that these species are not favored on silica [46]. Results from DFT calculations for CO on Rh(111) give a vibrational frequency of 2072 cm^{-1}, which is in agreement with the experimental observation. Infrared spectra of CO adsorbed on 3% $Rh/0.9Te/SiO_2$ at 203 K show bands at 2057 and 2031 cm^{-1}. Similarly, spectra of CO adsorbed on 3% $Rh/0.7Te/SiO_2$ at 203 K show a band at 2022 cm^{-1} with a shoulder at 2051 cm^{-1}. The absence of multi/bridge-bonded CO on the Rh–Te catalysts is again evidence that the surface contains significant amounts of Te. Results from DFT calculations for CO on the fcc and hcp sites (with the Rh atom lifted above the surface) of the Te-terminated RhTe(0001) surface give C–O stretching frequencies of 2105 and 1974 cm^{-1}, respectively. We now assign the experimentally observed band at 2031 cm^{-1} for 3% $Rh/0.9Te/SiO_2$ and band at 2022 cm^{-1} for 3% $Rh/0.7Te/SiO_2$ to CO adsorbed on sites similar to the hcp site of the Te-terminated RhTe(0001) surface. We do not believe that the weaker band at ~ 2050 cm^{-1} is caused by CO adsorbed on sites similar to the fcc site of the Te-terminated RhTe(0001) surface, because bonding of CO on this site is calculated to be very weak (-14 kJ/mol). Instead, we suggest that the less intense band near 2050 cm^{-1} is due to CO adsorbed on a different facet of RhTe alloy or to RhTe particles having slightly different Rh–Te atomic ratios. We note that the lower IR frequencies of CO adsorbed on the Rh–Te catalysts compared to Rh/SiO_2 may also be partially caused by less significant dipole–dipole coupling between neighboring CO molecules, in view of the larger separation between adsorbates on the Rh–Te catalysts.

We attribute the increase in the intensities of the CO bands in IR spectra collected at 303 versus 203 K on the 3% $Rh/0.9Te/SiO_2$ and 3% $Rh/0.7Te/SiO_2$ catalysts to CO-induced surface reconstruction, i.e., movement of a Rh atom from the second layer to the surface as calculated for the Te-terminated RhTe(0001) surface. In particular, an increase in intensity of CO bands upon warming the sample from 203 to 303 K is not observed for the Rh/SiO_2 catalyst. In addition, the increase in intensity of the CO bands for the 3% $Rh/0.7Te/SiO_2$ sample is not reversible when the sample is subsequently cooled to 203 K. Instead, the IR results suggest that the surface of RhTe catalysts undergo an irreversible surface reconstruction when the catalysts are warmed from 203 to 303 K in the presence of 3 Torr of CO. We note that in a similar way, adsorbate-enhanced surface self-diffusion of Pt atoms was observed on the Pt(110) surface [47].

We have estimated from the results of our DFT calculations that the activation energy barrier for CO-induced surface reconstruction near the hcp site of Te-terminated RhTe(0001) is at least 44 kJ/mol. Based on the results from IR experiments, we assume the rate constants for surface reconstruction at 203 and 303 K are $< 10^{-4}$ s^{-1} and > 1 s^{-1}, respectively. Using a normal preexponential factor of 10^{13} s^{-1}, the activation energy barrier for CO-induced surface reconstruction is then estimated to be about 68–74 kJ/mol, which is consistent with the lower limit for this barrier (44 kJ/mol) estimated from our DFT calculations. Therefore, it is likely that CO-induced reconstruction would not be significant at 203 K (for the experimental times of the present study), but this reconstruction would take place readily at 303 K in the presence of CO. The higher intensity of the IR bands for adsorbed CO on the reconstructed surfaces of the $Rh/Te/SiO_2$ catalysts (compared to the situation where the samples are exposed to CO at 203 K) would suggest that the extinction coefficient for IR absorbance is higher for CO adsorbed on reconstructed surfaces.

The microcalorimetric measurements on the 3% $Rh/0.9Te/SiO_2$ sample at 203, 253, and 303 K also provide evidence for the presence of CO-induced surface reconstruction between 203 and 303 K. In particular, the heat of CO adsorption measured at 253 and 303 K is higher than that measured at 203 K for all coverages, and the difference in heat of adsorption increases to ~ 20 kJ/mol as the coverage increases. Given the moderate heat of adsorption measured, the dosed CO molecules should be well equilibrated with the surface, as confirmed by the observation that the heat of adsorption is not constant (i.e., not equal to a constant average value) with increasing surface coverage. In fact, results from DFT studies of CO adsorption on hcp sites of Te-terminated RhTe(0001) with a 3×3 unit cell show that CO-induced surface reconstruction leads to an increase in the strength of CO adsorption by 17 kJ/mol. We note that at all three tempera-

tures, the heat of adsorption continuously decreases with increasing uptake on 3% $Rh/0.9Te/SiO_2$. As shown by DFT calculations on hcp sites of Te-terminated RhTe(0001), the adsorption of CO pulls the underlying Rh atom to the surface and pushes away the three-fold Te atoms of the hcp site, which may weaken the bonding of CO at neighboring sites.

The activation energy barrier for O-induced surface reconstruction is predicted to be 44 kJ/mol. This relatively low activation energy barrier for the pulling of Rh atoms from the second layer to the surface may be related to the experimental observation that Rh–Te-based catalysts are not stable during the oxidative diacetoxylation of 1,3-butadiene (at 353 K). Specifically, Rh atoms may be pulled to the surface, followed by elution into the aqueous solution of acetic acid.

5. Conclusions

Results from microcalorimetric measurements show that CO adsorbs on Rh/SiO_2 with an initial heat of 160 kJ/mol. The addition of Te to Rh, leading to a $Rh/0.9Te/SiO_2$ sample, decreases the initial heat of CO adsorption to about 87 kJ/mol. Also, addition of Te to form this Rh–Te catalyst decreases the saturation uptake of CO to a value that is 20% of the update on a Rh/SiO_2 with the same Rh loading (3 wt%).

Results from DFT studies for CO adsorption on Rh(111), Rh-terminated RhTe(0001), and RhTe($11\bar{2}0$) show strong adsorption on all surfaces (i.e., heats higher than 160 kJ/mol). In contrast, weaker adsorption was calculated for adsorption of CO on Te-terminated RhTe(0001) surfaces. Comparing the effect of Te predicted by DFT calculations with microcalorimetric results, and given the lower surface energy of Te, it thus appears that the surface of a $Rh/0.9Te/SiO_2$ catalyst is most likely a Te-enriched surface. On the Te-terminated RhTe(0001) surface, the hcp site (atop site for Rh atoms of the second layer) is more favorable than the fcc site (three-fold hollow site for Rh atoms of the second layer) by 44 kJ/mol. The heat of CO adsorption on the hcp site is predicted to be 69 kJ/mol when the Rh atom is pulled out to the surface by a CO-induced surface reconstruction, which is 17 kJ/mol more stable compared to the situation when the Rh atom is still below surface Te layer. The activation energy barrier for this CO-induced surface reconstruction is estimated to be at least 44 kJ/mol, based on results for O-induced surface reconstruction.

Infrared spectra for CO adsorbed on the 3% $Rh/0.9Te/SiO_2$ and 3% $Rh/0.7Te/SiO_2$ samples show bands at 2031 and 2022 cm^{-1}, respectively, and these values are lower than the frequency of 2080 cm^{-1} observed for CO on Rh/SiO_2. Results from DFT calculations indicate that the C–O stretching frequency is lower for CO adsorbed on the hcp site of the Te-terminated RhTe(0001) surface compared to CO on the atop sites of Rh(111), i.e., 1974 versus 2072 cm^{-1}, respectively. Accordingly, the experimentally observed IR band for CO on 3% $Rh/Te/SiO_2$ catalysts is assigned to CO adsorbed on sites similar to the hcp site of the Te-terminated RhTe(0001) surface. In addition, we suggest that the CO-induced surface reconstruction, as predicted in DFT calculations, causes the increase in the intensity of the IR band for adsorbed CO when the $Rh/Te/SiO_2$ samples are warmed from 203 to 303 K in the presence of CO.

Acknowledgment

We acknowledge funding from the Mitsubishi Chemical Corporation.

References

[1] Y. Hara, H. Kusaka, H. Ohno, M. Okuda, EP Patent 904836, 1999.
[2] K. Takehira, H. Mimoun, I. Seree De Roch, J. Catal. 58 (1979) 155.
[3] K. Takehira, J.A.T. Chena, S. Niwa, T. Hayakawa, T. Ishikawa, J. Catal. 76 (1982) 354.
[4] A.V. Devekki, N.V. Trushova, M.I. Yakushkin, Neftekhimiya 31 (1991) 37.
[5] Y. Takayama, S. Saito, U. Yoshizawa, Y. Ishii, JP Patent 45026850, 1970.
[6] M. Ono, Y. Tsunematsu, JP Patent 11315049, 1999.
[7] D. Laucher, M. Costantini, EP Patent 462031, 1991.
[8] M.A. Leiber, J.R. Ebner, K.-T. Wan, A. Woods, P.E. Rogers, WO Patent 0146208, 2001.
[9] J. Shen, J.M. Hill, R.M. Watwe, B.E. Spiewak, J.A. Dumesic, J. Phys. Chem. 103 (1999) 3923.
[10] J.M. Hill, R. Alcala, R.M. Watwe, J.Y. Shen, J.A. Dumesic, Catal. Lett. 68 (2000) 129.
[11] J.M. Hill, J.Y. Shen, R.M. Watwe, J.A. Dumesic, Langmuir 16 (2000) 2213.
[12] M. Smedh, A. Beutler, M. Borg, R. Nyholm, J.N. Andersen, Surf. Sci. 491 (2001) 115.
[13] A. Beutler, E. Lundgren, R. Nyholm, J.N. Andersen, B.J. Setlik, D. Heskett, Surf. Sci. 396 (1998) 117.
[14] P. Cernota, K. Rider, H.A. Yoon, M. Salmeron, G. Somorjai, Surf. Sci. 445 (2000) 249.
[15] R. Linke, D. Curulla, M.J.P. Hopstaken, J.W. Niemantsverdriet, J. Chem. Phys. 115 (2001) 8209.
[16] M. Mavrikakis, M. Baumer, H.-J. Freund, J.K. Nørskov, Catal. Lett. 81 (2002) 153.
[17] M. Mavrikakis, J. Rempel, J. Greeley, L.B. Hansen, J.K. Nørskov, J. Chem. Phys. 117 (2002) 6737.
[18] P.J. Feibelman, B. Hammer, J.K. Nørskov, F. Wagner, M. Scheffler, R. Stumpf, R. Watwe, J.A. Dumesic, J. Phys. Chem. B 105 (2001) 4018.
[19] M. Frank, R. Kuhnemuth, M. Baumer, H.-J. Freund, Surf. Sci. 427–428 (1999) 288.
[20] S. Trautmann, M. Baerns, J. Catal. 150 (1994) 335.
[21] F. Solymosi, H. Knoezinger, J. Chem. Soc. Faraday Trans. 86 (1990) 389.
[22] D.A. Buchanan, M.E. Hernanadez, F. Solymosi, J.M. White, J. Catal. 125 (1990) 456.
[23] S.D. Worley, C.A. Rice, G.A. Mattson, C.W. Curtis, J.A. Guin, A.R. Tarrer, J. Phys. Chem. 86 (1982) 2714.
[24] A. Erdohelyi, F. Solymosi, J. Catal. 84 (1983) 446.
[25] M. Frank, S. Andersson, J. Libuda, S. Stempel, A. Sandell, B. Brena, A. Giertz, P.A. Bruhwiler, M. Baumer, N. Martensson, H.-J. Freund, Chem. Phys. Lett. 310 (1999) 229.

[26] A. Berko, G. Menesi, F. Solymosi, J. Phys. Chem. 100 (1996) 17,732.
[27] B.E. Spiewak, J. Shen, J.A. Dumesic, J. Phys. Chem. 99 (1995) 17,640.
[28] B.E. Spiewak, J.A. Dumesic, Thermochim. Acta 290 (1997) 43.
[29] Z. Ding, H. Kleykamp, F. Thmmler, J. Nucl. Mater. 171 (1990) 134.
[30] J. Neugebauer, M. Scheffler, Phys. Rev. B 46 (1992) 16,067.
[31] D.R. Lide (Ed.), CRC Handbook of Chemistry and Physics, 76th ed., CRC Press, Boca Raton, FL, 1996.
[32] S. Geller, J. Am. Chem. Soc. 77 (1955) 2641.
[33] B. Hammer, L.B. Hansen, J.K. Nørskov, Phys. Rev. B 59 (1999) 7413.
[34] D. Vanderbilt, Phys. Rev. B 41 (1990) 7892.
[35] J.A. White, D.M. Bird, Phys. Rev. B 50 (1994) 4954.
[36] J.P. Perdew, J.A. Chevary, S.H. Vosko, K.A. Jackson, M.R. Pederson, D.J. Singh, C. Fiolhais, Phys. Rev. B 46 (1992) 6671.
[37] G. Kresse, J. Furthmuller, Comput. Mater. Sci. 6 (1996) 15.
[38] Y. Xu, M. Mavrikakis, Surf. Sci. 494 (2001) 131.
[39] N. Brønsted, Chem. Rev. 5 (1928) 231.
[40] M.G. Evans, N.P. Polanyi, Trans. Faraday Soc. 34 (1938) 11.
[41] D.H. Wei, D.C. Skelton, S.D. Kevan, Surf. Sci. 381 (1997) 49.
[42] C.J. Zhang, P. Hu, M.-H. Lee, Surf. Sci. 432 (1999) 305.
[43] J.A. Dean (Ed.), Lange's Handbook of Chemistry, 15th ed., McGraw–Hill, New York, 1999.
[44] J.T. Yates Jr., E.D. Williams, W.H. Weinberg, Surf. Sci. 91 (1980) 562.
[45] M. Mavrikakis, B. Hammer, J.K. Nørskov, Phys. Rev. Lett. 81 (1998) 2819.
[46] F. Solymosi, M. Pasztor, G. Rakhely, J. Catal. 110 (1988) 413.
[47] S. Horch, H.T. Lorensen, S. Helveg, E. Laegsgaard, I. Stensgaard, K.W. Jacobsen, J.K. Nørskov, F. Besenbacher, Nature 398 (1999) 134.